

Angle-dependent infrared reflectance measurements in support of VIIRS

Simon G. Kaplan, Enrique J. Iglesias^{*}, and Leonard M. Hanssen

National Institute of Standards and Technology, Gaithersburg, MD 20899

ABSTRACT

We have developed a goniometric reflectometer using a Fourier-transform infrared (FTIR) spectrometer source for polarized reflectance measurements from 1 μm to 20 μm wavelength at angles of incidence from 10° to 80°, with an incident beam geometry of approximately $f/25$. Measurements are performed in either absolute mode, or relative to a reference mirror that has been calibrated at near-normal incidence using an integrating sphere-based reflectometer. Uncertainties in the 0.2 % to 0.5 % range are achieved using a photoconductive 77 K InSb detector from 1 μm to 5 μm and a 12 K Si:As BIB detector from 2 μm to 20 μm . The performance of the system has been tested using dielectric materials such as Si as well as high-quality Au mirrors. We describe measurements of SiO_x-coated Ag mirrors to assess their performance for such applications as the half-angle mirror (HAM) in the VIIRS optical scanning system. Various coatings are analyzed to help assess the effect of p-polarized absorption bands at angles of incidence from 10° to 65° and wavelengths between 3 μm and 13 μm .

Keywords: infrared, optical coatings, polarization, radiometry, reflectance

1. INTRODUCTION

The spectral reflectance of coated optical components such as windows, filters, and mirrors can be an important factor in the calibration of remote sensing systems [1]. Coatings are usually designed to either minimize the reflectance in a given waveband, for windows or filters, or to provide very high reflectance with low loss, as for dielectric mirrors [2]. In addition, windows or mirrors are often coated with a protective layer to resist degradation. Such layers are designed to have minimal impact on the optical performance of the uncoated component. While the absorption loss in these films can be modeled using handbook values for the optical constants of their constituents, the actual properties of a vacuum-deposited thin film can vary substantially depending on the deposition conditions and subsequent environmental exposure [3]. This variability can be especially pronounced for large angles of incidence with p-polarized illumination [4]. It thus becomes necessary to accurately characterize the optical performance of the coated artifact over the relevant range of wavelength, angle of incidence, polarization, and temperature in which it will be used.

An example of such an optical component is the half-angle mirror (HAM) which is part of the scanning system for the Visible/Infrared Imager/Radiometer Suite (VIIRS) instrument being built for the National Polar-Orbiting Operational Environmental Satellite System (NPOESS) [5]. The mirror is required to have high reflectance over the reflected solar (400 nm to 2500 nm) as well as the thermal infrared (2.5 μm to 12.5 μm) spectral regions. While the exact composition of the protective coating is proprietary to the vendor, we chose to use SiO_x with H₂O as a model system. Because the angle of incidence on the HAM varies over the scanning range of the instrument, it is necessary to understand the variation in its reflectance versus incident angle and polarization for use in instruments such as VIIRS.

In this paper we describe measurements of the angle- and polarization-dependent reflectance of several coated mirror samples. The measurements were made using a goniometer-based reflectometer in conjunction with an FTIR spectrometer whose design has been reported previously [6, 7]. The major recent upgrade to this facility has been the addition of a liquid helium-cooled Si:As Blocked Impurity Band (BIB) detector [8] to extend its wavelength range out to 30 μm in principle. The performance of the reflectometer using this detector is analyzed with an assessment of uncertainties in the measurement, and the measured reflectance data are compared to expected values for Au and Ag mirrors using handbook values for the optical constants of the coatings.

^{*} Permanent address: Physics Department, Universidad Simón Bolívar, Caracas, Venezuela 1089

2. EXPERIMENTAL DETAILS

2.1 Optical setup of reflectance measurement

The optical layout of the goniometer/reflectometer system [6] is shown in Figure 1 below. The 50 mm diameter collimated ($\approx f/50$) output beam from the FTIR spectrometer is collected by a 90° off-axis paraboloidal (OAP) mirror with a reflected effective focal length of 200 mm and focused at $f/4$ onto a variable aperture plate. The diverging beam from the aperture is then collected by a second 90° OAP, which is positioned to project a slowly converging beam into the rest of the system. Two flat steering mirrors are used to align the beam to pass through the rotation axis of the goniometer, perpendicular to the plane of the sample surface. An opaque half-block is placed in the beam before the first OAP in order to remove inter-reflections between the FTIR and other components in the system, and the beam waist is reduced with an additional aperture yielding an $\approx f/25$ geometry at the sample position. For the measurements described here, the apertures were arranged to produce a 6 mm spot diameter at the sample surface.

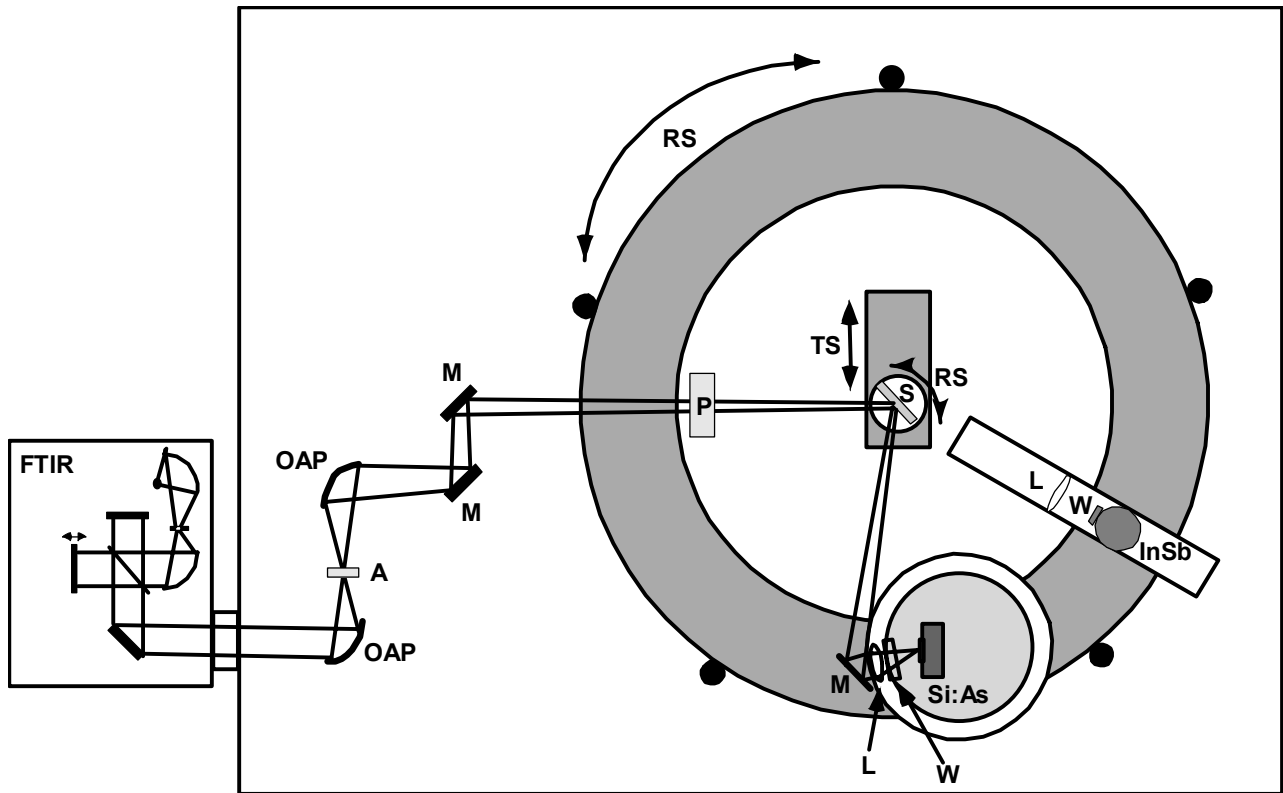


Figure 1. Optical layout of the goniometric reflectometer system described in text. OAP, 90° off-axis paraboloidal mirror; A, variable aperture plate; M, folding mirror; P, polarizer; RS, rotation stage; TS, translation stage; S, sample; L, lens; W, vacuum window. Also shown are the Si:As BIB and InSb photodetectors. The FTIR spectrometer and reflectometer setups are housed in separate sealed enclosures purged with dry, CO_2 -free air.

The input beam is polarized using a wire-grid polarizer on a ZnSe substrate, with extinction coefficient < 0.005 over the $2\ \mu\text{m}$ to $20\ \mu\text{m}$ spectral region. The sample is front-surface mounted on a slotted sample holder designed to allow optical access up to 70° incidence. Manual tilt and translation stages are used to bring the surface plane of the sample onto the axis of the motorized sample rotation stage and perpendicular to the incident beam within $\pm 0.3^\circ$ to define normal incidence. Precision alignment of the reflectometer is done using the visible output beam of the FTIR spectrometer, making small adjustments in the sample holder tilt and translation along the beam direction to ensure that the reflected spot strikes the detector within $\approx 0.2\ \text{mm}$ of the same place as the straight through beam with the sample

removed from the path. The relative alignment of the inner and outer goniometer stages is controlled using a small diode laser and quadrant detector system. Once the system is aligned, reflectance data are obtained by ratioing the spectra obtained from the FTIR with the beam reflected from the sample to the spectra recorded with the sample out of the beam path.

2.2 Detector system design

For the 1 μm to 5 μm spectral region, the beam passes through a CaF_2 plano-convex lens and CaF_2 window onto a 3.5 mm diameter 77 K photoconductive InSb detector. For the 2 μm to 20 μm spectral region, the beam is reflected through a ZnSe lens and NaCl window onto a 3.1 mm x 3.1 mm photoconductive Si:As BIB detector housed in a liquid helium-cooled cryostat and maintained at a temperature of 12 K. A cooled NiCr-coated Ge neutral density filter with a transmittance of ≈ 0.001 is placed in front of the BIB detector to attenuate the thermal background radiation and keep the response within the linear regime. In each case, the spot diameter on the detector is approximately 2 mm. Both detectors are tilted by 10° relative to the input beam to avoid inter-reflections with the spectrometer. The photoconductor signals are fed through a low-noise current pre-amplifier and back into the FTIR for data collection and Fourier processing.

Figure 2 below shows a photograph of the two detector cryostat systems mounted on the motorized outer rotation stage of the goniometer. When filled with cryogens, the InSb and BIB detector cryostats are able to maintain the detector temperatures for approximately 30 h and 48 h, respectively. Also visible in Figure 2 is the two-axis translation stage and rotary table on which the BIB detector cryostat is mounted. This is used to manually position the detector relative to the input beam.

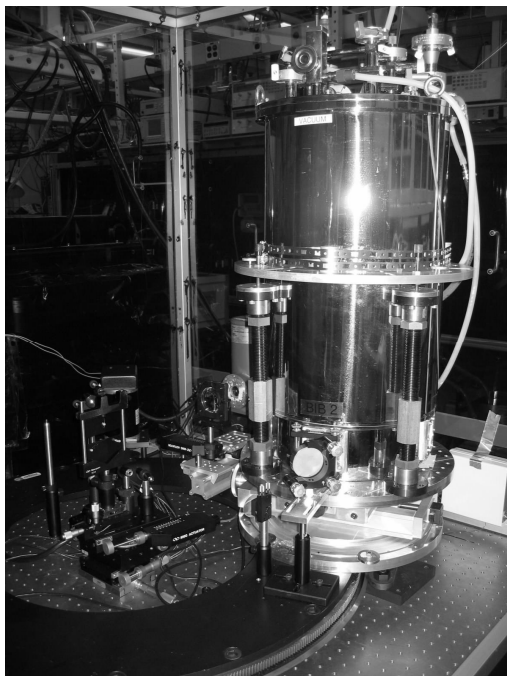


Figure 2. Photograph of goniometer showing the two detector cryostats mounted on the outer rotation stage. The small InSb detector system is visible behind and to the left of the 50 cm tall liquid-He cryostat housing the Si:As BIB detector.

As has been discussed previously [6], the spatial uniformity of the detector is often the most important factor limiting the accuracy of absolute reflectance measurements such as these. Small unintentional beam motion or changes in beam geometry at the detector position between the sample and reference configurations can lead to errors in the ratioed reflectance spectrum due to nonuniformity in the detector response. While the nonuniformity of InSb detectors can be

quite low ($\approx 0.5\%$ over 1 cm diameter), the HgCdTe detectors used for longer wavelengths typically have much larger nonuniformity ($\approx 50\%$), and are thus of limited use in a high-accuracy reflectometer without some kind of averaging device such as an integrating sphere [9]. However, Si:As BIB detectors can be quite uniform [8]. Figure 3 shows a map of the relative responsivity of our BIB detector produced by recording the FTIR interferogram peak signal as the cryostat is translated in the plane perpendicular to the incident beam, with a focal spot size of $\approx 1.2\text{ mm} \times 1.6\text{ mm}$. It represents a spectral average over the $2\text{ }\mu\text{m}$ to $25\text{ }\mu\text{m}$ wavelength range present in the modulated FTIR output flux. From these data we infer a relative spatial nonuniformity of $\pm 1.5\%$ over the central $2\text{ mm} \times 2\text{ mm}$ area with an expanded uncertainty of $\pm 1\%$ (in this report we use a coverage factor of 2.) This includes any nonuniformities in transmittance of the vacuum window and neutral-density filter in front of the detector element itself.

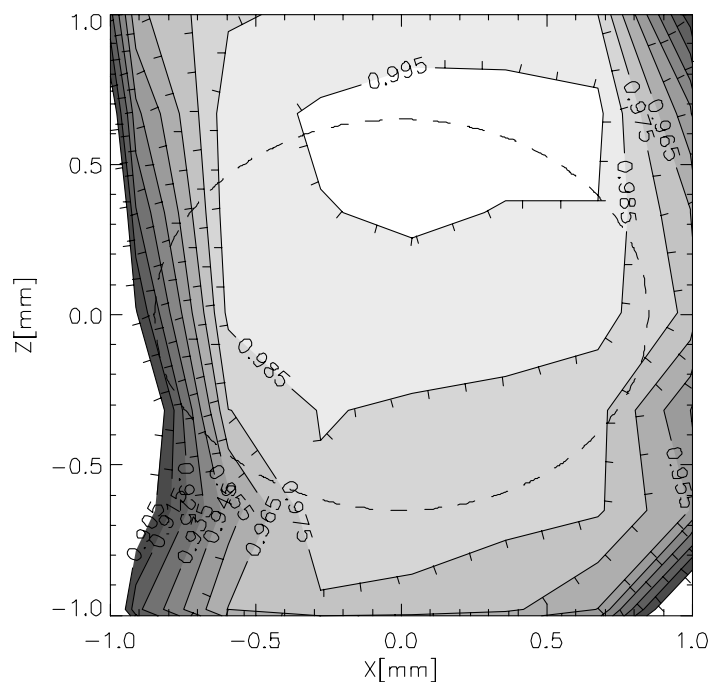


Figure 3. Spatial uniformity map of Si:As BIB detector system, showing the spectrally averaged responsivity variation for the FTIR output beam over the central $2\text{ mm} \times 2\text{ mm}$ area, along with the fitted beam profile (dashed line).

2.3 Measurement procedures

For the reflectance measurements in this study, the FTIR spectrometer was equipped with a ceramic-coated global source and a Ge-coated KBr beamsplitter. The external aperture in Figure 1 was set to 1.25 mm diameter. The spectrometer was scanned with a 20 kHz modulation rate for the reference HeNe laser (15800 cm^{-1} wavenumber) with a spectral resolution of 16 cm^{-1} and boxcar apodization. 1500 scans were averaged for each sample or reference spectrum, and the sequence of measurements was repeated to reduce the effects of drift in the modulated FTIR spectra or in the detector responsivity. Data were acquired with both the InSb and Si:As BIB detector systems, with a range of incident angles from 10° to 65° and both s- and p- polarization. The total averaging time for each angle and polarization was approximately 20 min. The sample temperature was near ambient ($22\text{ }^\circ\text{C}$).

In addition, the mirror samples were measured over the $2\text{ }\mu\text{m}$ to $16\text{ }\mu\text{m}$ wavelength range using a side sample-mount 150 mm diameter roughened Au-coated integrating sphere reflectometer attached to the same FTIR spectrometer [9]. In these measurements, the angle of incidence was fixed at 8° , with an $f/6$ focusing geometry. The detector is a 6 mm diameter 77 K HgCdTe photoconductor with a lens/concentrator combination to limit its field of view to an area on the bottom of the integrating sphere. A similar wire-grid polarizer was used to define s- and p-polarization. 16 measurement cycles were performed over a 6 hour time period at 8 cm^{-1} resolution. These near-normal incidence data have an expanded relative uncertainty of 0.3% and are used to normalize the angle-dependent measurements using the goniometer.

3. RESULTS AND DISCUSSION

3.1 SiO_x-coated Ag mirror samples

Figure 4 shows a comparison of near-normal incidence reflectance values for a 50.8 mm diameter SiO_x-coated Ag mirror sample using the integrating sphere and goniometer reflectometers. For this metallic mirror sample, Fresnel calculations predict that the differences in reflectance values between the 8° (sphere) and 10° (goniometer) incident angles are less than 0.0005, considerably smaller than the systematic (type-B) uncertainties in the measurements. Thus a comparison of the measurement results is useful. First of all, the sphere measurement results show a very high reflectance value, near the limit of what can be achieved with a metallic mirror in this spectral region. Absorption features near 3 μm, associated with H₂O, can be seen in both the s- and p-polarized spectra. A band centered near 9 μm due to the Si-O stretching mode is stronger in the p-polarized spectrum.

Comparing to the goniometer results, we see that there is good agreement between the sphere data and the goniometer data taken with the InSb detector; the differences are less than the uncertainties in the sphere measurements alone. However, the results taken with the BIB detector are 1 % to 1.5 % lower. In addition there are baseline slope and oscillations that appear to be due to Fabry-Perot fringes in the detector element, which are stronger in the s-polarized data. On the other hand, the angular dependence of the reflectance values obtained with the two detector systems over the 2 μm to 5 μm spectral region agrees to within 0.15 %. Also, the baseline slope and oscillations in the BIB data are independent of the angle of incidence. It therefore appears that most of the error in the BIB detector data is due to the mirror image flip between the sample and reference geometries. Nonuniformity in the input beam due to spatial variation in the source, beamsplitter, polarizer, and focusing optics is convolved with the nonuniform detector response shown in Figure 3. Small changes in detector position (~ 0.1 mm) in the focal plane have confirmed the smaller residual error due to beam motions on the detector over the range of incident angles in the goniometer. Thus the goniometer is capable of yielding much lower uncertainty in the relative angular dependence of the reflectance than in the absolute reflectance value itself.

We thus use the near-normal incidence data acquired with the sphere reflectometer to produce corrected angle-dependent reflectance spectra for each incident angle, θ

$$R(\theta) = \frac{R_{gonio}(\theta)}{R_{gonio}(10^\circ)} \cdot R_{sphere} \quad (1)$$

Where R_{gonio} and R_{sphere} are the absolute reflectance spectra obtained with the goniometer and sphere, respectively. The results of this procedure are shown in Figures 5(a) and 5(c), where the spectral resolution has also been reduced to 32 cm⁻¹.

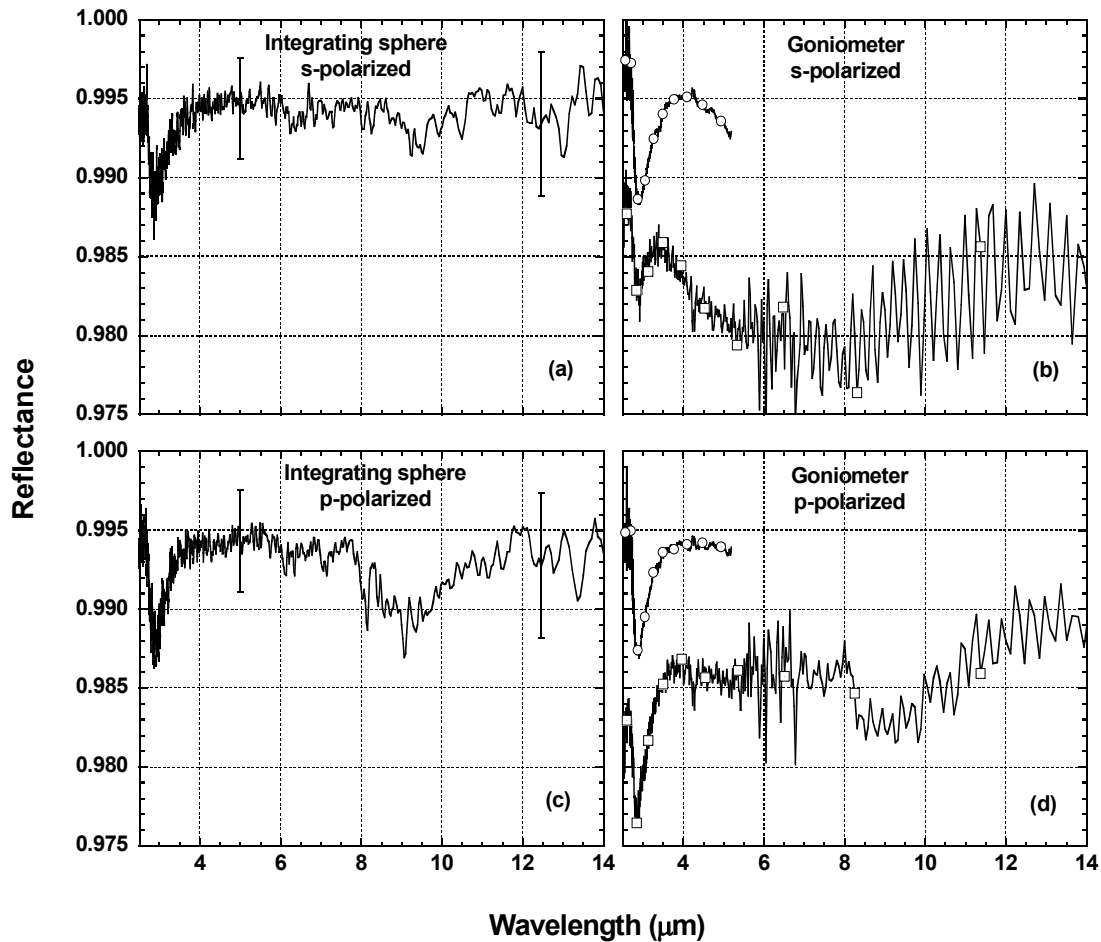


Figure 4. Comparison of near-normal incidence reflectance data for a 50.8 mm diameter SiO_x -coated Ag mirror sample taken with the integrating sphere and goniometer setups. In frames (b) and (d), the circles represent measurements with the InSb detector and the squares measurements taken with the Si:As BIB detector. Representative error bars are displayed for the expanded uncertainty (coverage factor 2) in the sphere reflectance measurements.

Also shown in Figure 5(a) is the expanded uncertainty in reflectance, including both type A and type B components from the relative goniometer measurement combined with the uncertainty of the absolute sphere measurement. An increase of ≈ 0.004 is seen in the s-polarized spectra as the incident angle is changed from 10° to 65° , whereas the p-polarized spectra show stronger absorption in the bands near $3 \mu\text{m}$ and $9 \mu\text{m}$ as the incident angle is increased.

In order to independently assess the quality of the reflectance data and of the mirror sample, we compare the measured results with calculated curves for a model system consisting of a SiO_2 film with H_2O inclusions on a substrate of Ag. Values for the optical constants of these constituents are taken from handbook data [10]. While the actual microstructure of vacuum-deposited SiO_x films is very sensitive to deposition conditions, other researchers have had some success with this simplified model of a porous silica film [11, 12]. Uptake of water in the film presumably leads to production of SiOH as well, which yields additional absorption bands that are not accounted for in this model. The dielectric function ϵ_f of the silica film can be modeled using the Bruggeman effective medium approximation [12] (EMA) as

$$(1 - f_w) \frac{\epsilon_s - \epsilon_f}{\epsilon_s + 2\epsilon_f} + f_w \frac{\epsilon_w - \epsilon_f}{\epsilon_w + 2\epsilon_f} = 0 \quad (2)$$

where ϵ_s and ϵ_w are the (complex) dielectric functions of SiO₂ and H₂O respectively, and f_w is the volume fraction of water in the film. In the Fresnel calculations for reflectance, the silica film is treated coherently, while the Ag substrate is treated incoherently [13] and assumed to be in the bulk (opaque) thickness limit, so its precise thickness is not important. The two free parameters used to fit the observed absorption strengths of the 3 μm and 9 μm features are the film thickness d and the water volume fraction f_w .

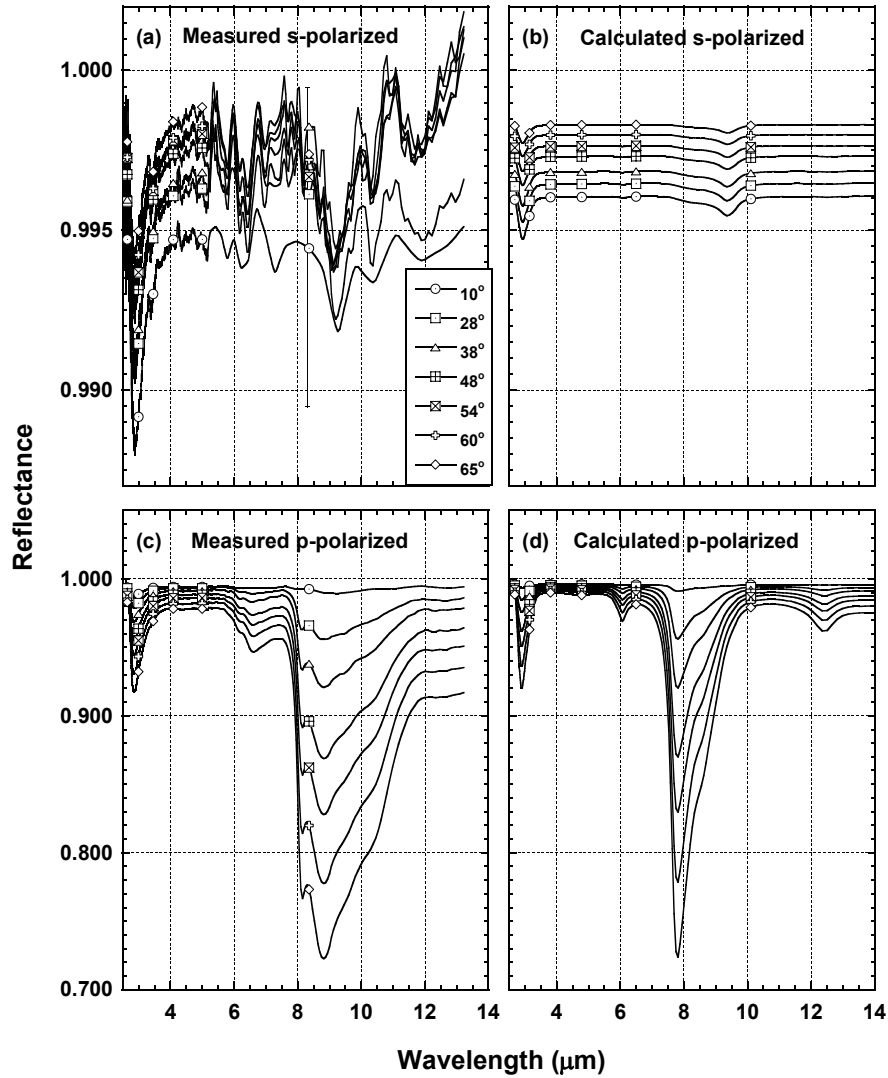


Figure 5. Comparison of measured reflectance values from 10° to 65° incidence for a 50.8 mm diameter coated Ag sample with calculations using handbook values for n and k of Ag, SiO₂, and H₂O, described in the text.

The values of the optical constants $n+ik = \sqrt{\epsilon}$ from the fit are shown in Figure 6, while the reflectance calculation results are shown in Figures 5(b) and 5(d). The best fit to the data is obtained with $d = 46$ nm and $f_w = 0.42$. Comparing the s-polarized data in Figures 5(a) and 5(b), we see that the measured reflectance curve for 10° incidence is only slightly lower (0.001) than the predicted values for Ag, although the absorption bands near $3 \mu\text{m}$ and $9 \mu\text{m}$ are stronger than predicted. The overall upward shift in measured reflectance as the incidence angle is increased is slightly larger than the predicted amount, and not as uniformly monotonic. However, the differences between the measured and predicted reflectances are within the uncertainty of the measured data. The s-polarized reflectance data are relatively insensitive to absorption bands in the silica film, and demonstrate the effectiveness of the protective layer in preserving the nearly ideal optical response of the Ag film in this frequency range.

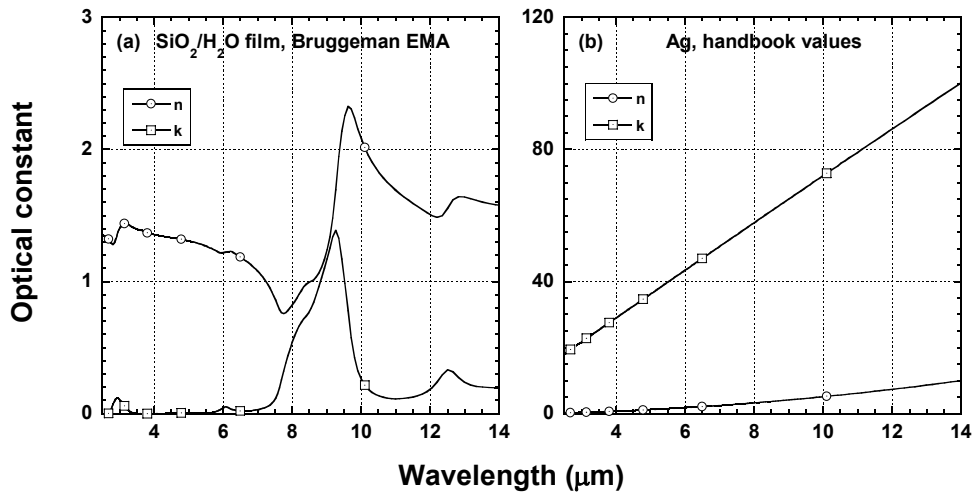


Figure 6. Optical constants used to produce the model reflectance values for the coated mirror sample shown in Figure 5. Frame (a) shows the effective medium n and k for the hydrated silica film, while frame (b) shows the handbook n and k values for Ag.

The p-polarized reflectance values shown in Figures 5(c) and 5(d) show good agreement between the measured and predicted change in absorption level as the incidence angle is increased. However, the measured absorption bands are significantly broader than the predicted ones, and are generally shifted toward longer wavelength. These differences are clearly larger than the expanded uncertainties in the reflectance data. This demonstrates the importance of measuring the reflectance of coated mirrors if accurate values are needed over a large range of angles of incidence. The effective optical constants of the thin silica film are very sensitive to composition, microstructure, and environmental exposure [3,11,12], and the p-polarized reflectance at large angles is very sensitive to dispersion in the effective n . A comparison of two test samples showed very similar reflectances near 0.995 for near-normal incidence, but several percent variation in the p-polarized absorption at larger angles of incidence.

3.2 Au mirror

An additional test of the performance of the goniometer is measuring the reflectance of a bare Au mirror. Figure 7(a) shows the measured reflectance from $2 \mu\text{m}$ to $5 \mu\text{m}$ wavelength of a 25.4 mm diameter electroplated Au mirror for three incident angles.

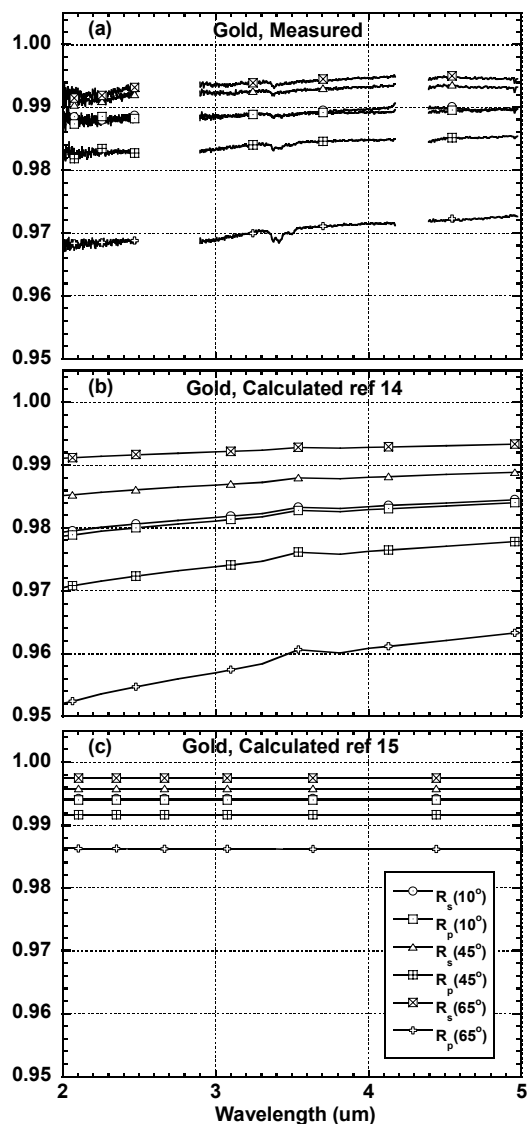


Figure 7. Comparison of measured reflectance values for a Au mirror with predicted values using two different sets of literature values for n and k of Au.

While the reflectance of 0.99 at near-normal incidence is not quite as high as that achieved by the protected Ag mirrors, there is no apparent H₂O-band absorption in the p-polarized data, with only the weak hydrocarbon absorption near 3.4 μm affecting the smooth variation of reflectance versus wavelength. The optical response of Au films is also very sensitive to deposition and environmental exposure conditions, although good quality films are very stable over time. In Figures 7(b) and 7(c) we show calculated reflectance of Au using two different sets of optical constants that can be found in handbooks [14,15]. The values in 7(b) are probably closer to typical commercially available gold mirrors, while those in 7(c) represent the best values obtained from fresh vacuum-deposited gold measured *in-situ* with an ellipsometer. The measured values in 7(a) fall between these two limits, showing very good results for an electroplated Au mirror.

4. CONCLUSIONS

We have demonstrated the use of an FTIR-based goniometric reflectometer to measure the angle, wavelength, and polarization dependent reflectance of metallic mirrors in the infrared spectral region with a relative expanded uncertainty

of 0.5 %. Testing of coated mirror samples consisting of Ag with a protective overlayer of SiO_x reveals stable high reflectance values from the visible through the thermal infrared spectrum. Strongly angle-dependent p-polarized absorption bands near 3 μm and 9 μm due to the silica coating were observed. The performance of the goniometer is currently being tested to the long-wavelength limit (≈ 30 μm) of the Si:As BIB detector system.

5. REFERENCES

1. R. A. Barnes, W. L. Barnes, C-H. Lyu, and J. M. Gales, "An overview of the Visible and Infrared Scanner radiometric calibration algorithm," *J. Atmos. Ocean. Tech.* **17**, 395-405 (2000).
2. H. A. Macleod, "Thin-film optical coating design," in *Thin Films for Optical Systems*, ed. F. R. Flory (Marcel Dekker Inc., New York, 1995), pp. 1-39.
3. J. Rivory, "Ellipsometric measurements," in *Thin Films for Optical Systems* ed. F. R. Flory (Marcel Dekker Inc., New York, 1995), pp. 319-327.
4. J. Workman, Jr., "Spectroscopy of solids," in *Applied Spectroscopy: A Compact Reference for Practitioners*, ed. by J. Workman, Jr. and A. W. Springsteen (Academic Press, San Diego, 1998), pp. 241-243.
5. An overview of the VIIRS instrument can be found at http://www.ipo.noaa.gov/Technology/viirs_summary.html, provided by NOAA Satellite and Information Service (2008).
6. S. G. Kaplan and L. M. Hanssen, "Angle-dependent absolute infrared reflectance and transmittance measurements," *Proc. SPIE* **4103**, 75-84 (2000).
7. S. G. Kaplan and L. M. Hanssen, "Silicon as a standard material for infrared reflectance and transmittance from 2 to 5 μm," *Infr. Phys. Tech.* **43**, 389-396 (2002).
8. E. J. Iglesias, A. W. Smith, and S. G. Kaplan, "A sensitive, spatially uniform photodetector for broadband infrared spectrophotometry," *Appl. Opt.* **47**, 2430-2436 (2008).
9. L. Hanssen, "Integrating-sphere system and method for absolute measurement of transmittance, reflectance, and absorbance of specular samples," *Appl. Opt.* **40**, 3196-3204 (2001).
10. Optical constants data for Ag and SiO₂ obtained from *OPTIMATR 2.1*, Johns Hopkins University/Applied Physics Laboratory and ARSoftware, Inc., Landover, MD (1993); data for H₂O obtained from M. R. Querry, D. M. Wieliczka, D. J. Segelstein, "Water (H₂O)," in *Handbook of Optical Constants of Solids II*, ed. E. D. Palik (Academic Press, San Diego 1998), pp.1059-1077.
11. A. Brunet-Bruneau, J. Rivory, B. Rafin, J. Y. Robic, and P. Chaton, "Infrared ellipsometry study of evaporated SiO₂ films: Matrix densification, porosity, water sorption," *J. Appl. Phys.* **82**, 1330-1335 (1997).
12. A. Goullet, C. Vallée, A. Granier, and G. Turban, "Optical spectroscopic analyses of OH incorporation in SiO₂ films deposited from O₂/tetraethoxysilane plasmas," *J. Vac. Sci. Technol. A* **18**, 2452-2458 (2000).
13. C. J. Gabriel and A. Nedoluha, "Transmittance and reflectance of systems of thin and thick layers," *J. Mod. Optics* **18**, 415-423 (1971); method extended to non-normal incidence following J. D. Jackson, *Classical Electrodynamics, Second Edition* (John Wiley and Sons, New York 1975), pp. 278-282.
14. D. W. Lynch and W. R. Hunter, in *Handbook of Optical Constants of Solids*, ed. E. D. Palik (Academic Press, San Diego 1998), pp. 286-295.
15. *OPTIMATR 2.1*, Johns Hopkins University/Applied Physics Laboratory and ARSoftware, Inc., Landover, MD (1993).